Microelectronic Engineering 87 (2010) 601–609

Contents lists available at ScienceDirect

Microelectronic Engineering

journal homepage: www.elsevier.com/locate/mee

Effects of aging time, strain rate and solder thickness on interfacial fracture behaviors of Sn–3Cu/Cu single crystal joints

H.F. Zou, Z.F. Zhang *

Shenyang National Laboratory for Materials Science, Institute of Metal Research, Chinese Academy of Sciences, Shenyang 110016, PR China

ARTICLE INFO

Article history:
Received 23 April 2009
Received in revised form 14 July 2009
Accepted 24 August 2009
Available online 29 August 2009

Keywords:
Sn–Cu solder
Interfacial strength
Intermetallic compounds
Ductile-to-brittle transition
Strain rate
Fracture

ABSTRACT

The effects of aging time, strain rate and solder thickness on fracture behaviors of Sn–3Cu/Cu single crystal joints were investigated. Experimental results showed that short aging time (less than 10 days) did not obviously affect the tensile strength and fracture behaviors of the solder joints. However, strain rate and solder thickness played significant roles in the strength and fracture behaviors of the solder joints. It was observed that these joints broke in a ductile manner at low strain rates with a rapid increase in the tensile strength, but displayed a brittle manner at high strain rates with a slow increase in the tensile strength. A model was proposed to explain such ductile-to-brittle transition between solder and intermetallic compounds. In addition, the solder joints broke in a ductile manner and presented a low tensile strength for the joints with thicker solder, but displayed a brittle manner and a higher tensile strength for the joints with thinner solder.

1. Introduction

In electronic packaging field, soldering not only provides the electronic connection, but also ensures the mechanical reliability of solder joints under the service conditions. However, environmental and health concerning the use of Pb in electronic packaging have promoted the development and understanding for the problem of lead-free solders [1,2], which requires to develop new alloys with low melting point for the replacement of Sn–Pb alloys. Many experiments were designed to investigate the properties of Sn–Pb, Sn–Ag and Sn–Cu solder joints [3–7]. It has been reported that except for wetting behavior, most mechanical properties of lead-free solders are better than those of Sn–Pb alloys [1]. Some experiments were designed to investigate the relationship between the strain rate and mechanical properties of lead-free solder joints [8,9]. Experimental results indicated that the shear strength of solders or solder joints has an approximately linear relationship with the effective logarithmic shear strain rate [8].

At present, these researchers mainly paid much attention to the mechanical reliability of Sn–Ag and Sn–Ag–Cu solders. Compared with a series of Sn–Ag solder, Sn–Cu solder has many advantages such as low-cost, prohibiting dissolution of Cu substrate and availability, especially for iron, dip and wave soldering operations [1,10]. But there are limited data about mechanical properties of Sn–Cu solder and its joint, especially for the effect of strain rate [10–12]. In the electronic packaging field, strain rate often plays an important role in the mechanical properties of the joints because joints encounter various strain rates in service such as accidental drops of cellular phones and personal digital assistants (PDAs) from different heights [13]. Therefore, it is necessary to investigate the relationship between strain rate and strength of Sn–3Cu/Cu joint as well as its fracture modes in detail.

Another problem is that many samples (such as ball grid array (BGA) and stick) are always designed to investigate the mechanical properties [8,12,13]. As a result, the solder thickness would be different used in different researchers. This may lead to completely different results under the same heat treatment and loading condition for different researchers. Therefore, the effect of the solder thickness on interfacial fracture behaviors of lead-free solder joints should be studied. In addition, it is very difficult to estimate the interfacial strength of the joint because fracture crack does not always propagate along the interface exactly between the solder and intermetallic compounds (IMCs) [12,13–15]. In the current study, we employ the Sn-3 wt%Cu/Cu joints as an example to reveal the effects of aging time, strain rate and solder thickness on the tensile fracture behaviors for a comprehensive understanding of the interfacial strength and failure mode of the lead-free solder joint.

2. Experimental procedure

In this study, single crystal Cu was used as a substrate and Sn–3Cu alloy was employed as a solder. Firstly, single crystal Cu plate with dimensions of $40 \times 150 \times 10\ mm^3$ was grown from Cu with a

* Corresponding author.
E-mail address: zhfzhang@imr.ac.cn (Z.F. Zhang).

0167-9317/$ - see front matter © 2009 Elsevier B.V. All rights reserved.
doi:10.1016/j.mee.2009.08.021

purity of 99.999% by the Bridgman method in a horizontal furnace. Secondly, Sn–3Cu was prepared by melting high purity (4N) Sn and Cu in vacuum (<10^{-1} Pa) at 800 °C for 30 min. The bonding surface of the single crystal Cu was detected to have an orientation of [358] by electron backscatter diffraction (EBSD) technique. This ensured that the formed IMC grains on the Cu single crystal with such orientation have random orientation and homogeneous size [16]. The single crystal Cu and Sn–3Cu were ground with 800#, 1000#, 2000# SiC paper and then carefully polished with the 2.5, 1.5 and 0.5 μm polishing pastes. Finally, the prepared samples were bonded in the oven with a constant temperature of 260 °C for 15 min. The as-reflowed samples were isothermally aged at 160 °C for 0, 2, 5, 10 days, respectively. After the solid-state aging, all the samples were carefully polished with polishing pastes. In order to investigate the relationship between aging time and tensile strength, some of samples were tested on an INSTRON 8871 testing machine with an average strain rate of about $8 \times 10^{-4}\ s^{-1}$ at room temperature in air. In addition, some samples aged for 5 days, with the dimensions of $50 \times 7 \times 2\ mm^3$ were used to investigate the relationship between strain rate and tensile strength of the solder joints. In this study, seven strain rates ranging from 4.2×10^{-5} to $2.4 \times 10^{-1}\ s^{-1}$ were employed and three samples were tested at each strain rate. Meanwhile, some samples were used to investigate the effect of solder thickness on the fracture mode. These samples were isothermally aged at 110 °C for 15 h and then were subjected to tensile test at an average strain rate of about $5 \times 10^{-4}\ s^{-1}$. All the fracture samples were observed to reveal the deformation and fracture morphology with a supra 35 LEO scanning electron microscope (SEM).

3. Results and discussion

3.1. Effect of aging time on tensile strength

Tensile stress–displacement curves and tensile strength–aging time curves of Cu/Sn–3Cu joints are shown in Fig. 1. It can be seen that the tensile strength of Sn–3Cu/Cu joints only has a slightly decrease with increasing aging time, as illustrated in Fig. 1b. The ultimate tensile strength only decreases about 5 MPa for the joint aging at 160 °C even for 10 days compared with the as-reflowed joints. The current strength variation with aging time is not consistent with Bae's results because they found that the shear strength would intensely decrease 25 MPa when aging at 180 °C for 7 days [15]. The reason might be that the deformation and fracture modes under shear test and their strain rate are different from us.

Fig. 2 shows the cross-section macroscopic fracture morphology of tensile samples aging at 160 °C for different days. It can be seen that there is little difference among them. For each facture cross-section, there is much solder clinging to Cu side. It is indicated that the fracture always occurred in the solder for all samples. However, the previous results reported that the transition of fracture mode was mainly induced by increasing aging time or electromigration [13,17], which was not observed in our experiment. It might be attributed to the relatively short aging time.

Fig. 3 shows the cross-section fracture morphology in detail of the samples aged at 160 °C for different days at a constant strain rate of $4.2 \times 10^{-4}\ s^{-1}$. There are some differences at the interface for the fracture cross-section of samples aged for different days. For the as-reflowed samples, some broken scallop-like Cu_6Sn_5 grains (as determined by the energy-dispersive spectrometer (EDS)) were detected at the interface, as displayed in Fig. 3a. It is similar to the previous results [17,18]. For the samples aged for 2 days, the morphology of IMCs gradually transformed from scallop-like to planar-type, which is similar to the previous studies [17,19,20], the crack propagated along the interface between Cu_6Sn_5 IMC and Sn–3Cu solder, as illustrated in Fig. 3b. Some slip bands were formed on the surface of Cu substrate. These slip bands would impinge upon the IMCs under tensile loading, and then vertical cracks initiated at the interface. As shown in Fig. 3c, the Cu_6Sn_5 layer has fallen off under tensile loading, which has been reported in the previous study [17]. It is indicated that most of cracks occurred initially within the interior of IMCs. With increasing tensile loading, those cracks propagated within the interior of IMC. However, when the samples were aged for 10 days, the cross-section fracture morphology is different from the former samples. Not only does Cu_6Sn_5 IMC fall off, but also some Cu_3Sn layer falls off Cu substrate. IMC layers were smashed during the tensile procedure, as displayed in Fig. 3d.

Fig. 4 shows the top view of the fracture interface of the samples aged for different days. Solder has been detected on the top view of the fracture interface for the as-reflowed samples, as indicated in Fig. 4a. Some dimples were detected in the samples aged for 2 days, but Cu–Sn IMC particles can not be observed in these dimples, as displayed in Fig. 4b. Compared with the samples aged for 2 days, the top view of the samples aged for 5 days is different. Many dimples, filled with IMC particles, were obviously detected, as illustrated in Fig. 4c. Some of these particles are identified as Cu_3Sn with the help of EDS. For the samples aged for 10 days, those dimples were not detected, but most of broken Cu_6Sn_5 particles were detected on the top view of the fracture interface, as indicated in Fig. 4d.

From the observations above, it can be concluded that the effect of aging time on the tensile strength and fracture mode is not significantly obvious in our experiments because the aging time is not long enough.

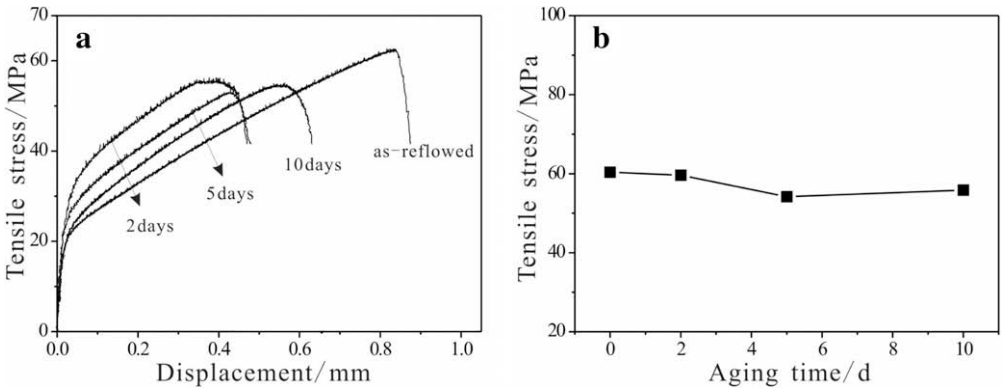

Fig. 1. Tensile stress–displacement curves and tensile strength–aging time curve of Sn–3Cu/Cu joints.

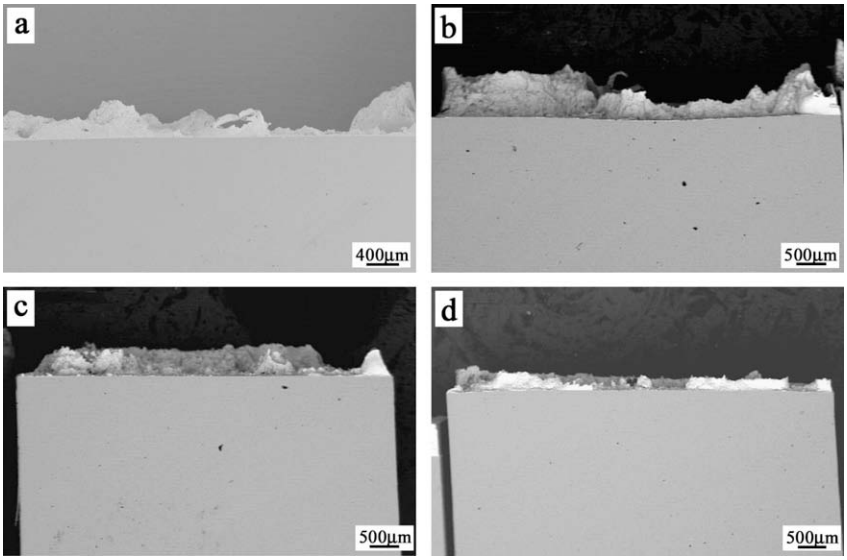

Fig. 2. Cross-section macroscopic fracture morphologies of tensile samples aged at 160 °C for (a) as-reflowed; (b) 2 days; (c) 5 days; and (d) 10 days at a constant strain rate of $4.2 \times 10^{-4}\ s^{-1}$.

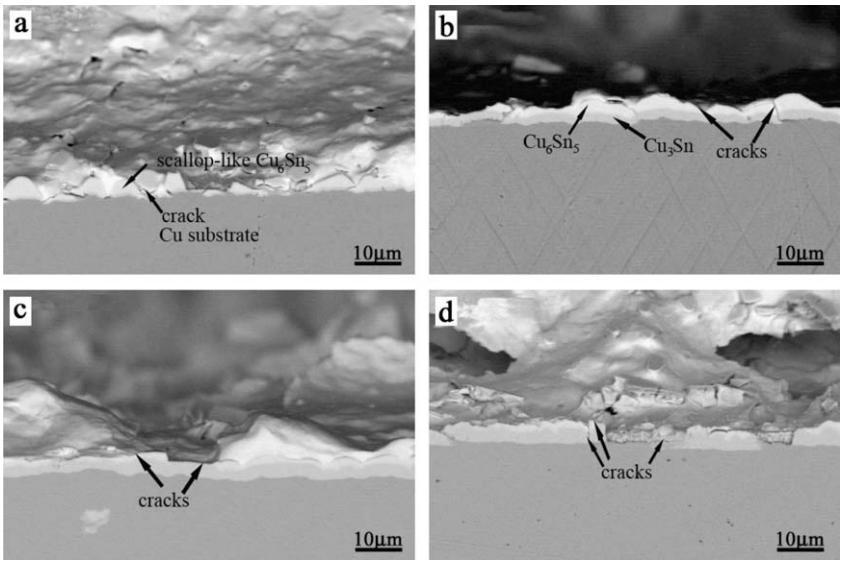

Fig. 3. Cross-section microscopic fracture morphologies of tensile samples aged at 160 °C for: (a) as-reflowed; (b) 2 days; (c) 5 days; and (d) 10 days at a constant strain rate of $4.2 \times 10^{-4}\ s^{-1}$.

3.2. Effect of strain rate on tensile strength

Many researchers have paid much attention to the effect of strain rate on the mechanical properties of bulk metallic materials [21,22], but the relationship between tensile strength of solder joints and strain rate has not been well investigated. Fig. 5a shows the typical tensile stress–strain curves of Cu/Sn–3Cu joints aged at 160 °C for 5 days at different strain rates. The tensile stress–strain curves demonstrate that the yielding, plastic flow and fracture behavior of the solder joint samples are similar to homogenous metallic materials. Fig. 5b shows the plot of the lg(strain rate)–lg(tensile strength) of the Cu/Sn–3Cu/Cu joints aged at 160 °C for 5 days. It is apparent that the tensile strength has a rapid increasing tendency with increasing strain rate. For example, the tensile fracture strength increases from 38.0 MPa at strain rate of $4.2 \times 10^{-5}\ s^{-1}$ to 72.1 MPa at strain rate of $2.4 \times 10^{-1}\ s^{-1}$. At the same time, it was also observed that the samples can display a higher tensile strain at higher strain rate, which was also observed in most of different metallic materials [21,22]. This phenomenon can be explained as follows: when the strain rate increases, work hardening effect will lead to much higher fracture strength of solder. That is to say the stress applied on copper will increase during the tensile process, which in return causes higher tensile plasticity of copper substrate.

Figs. 6 and 7 show the cross-section fracture morphologies of tensile samples aged at 160 °C for 5 days at different strain rates. There are many obvious differences. Figs. 6a and b and 7a and b are the cross-section fracture morphologies of tensile samples at strain rates of $4.2 \times 10^{-5}\ s^{-1}$ and $2.5 \times 10^{-3}\ s^{-1}$ (low strain rate). It is apparent that the micrograph of cross-section is very rough. Such phenomenon has been detected on many previous results [17,18]. However, compared with the low strain rate condition, the cross-section fracture morphologies of tensile samples at strain rates of $5.0 \times 10^{-2}\ s^{-1}$ and $2.4 \times 10^{-1}\ s^{-1}$ (high strain rate) are

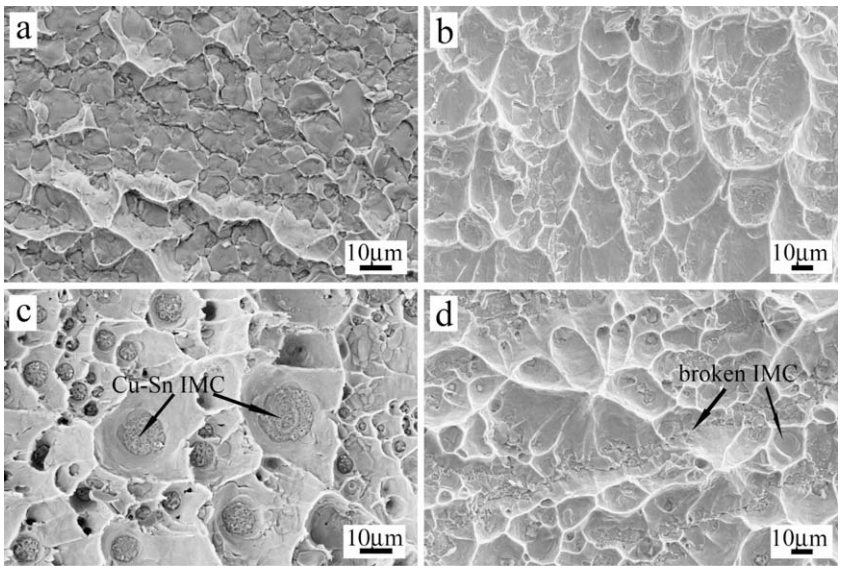

Fig. 4. The top view of the tensile fracture surfaces for the samples aged at 160 °C for: (a) as-reflowed; (b) 2 days; (c) 5 days; (d) 10 days at a constant strain rate of $4.2 \times 10^{-4}\ s^{-1}$.

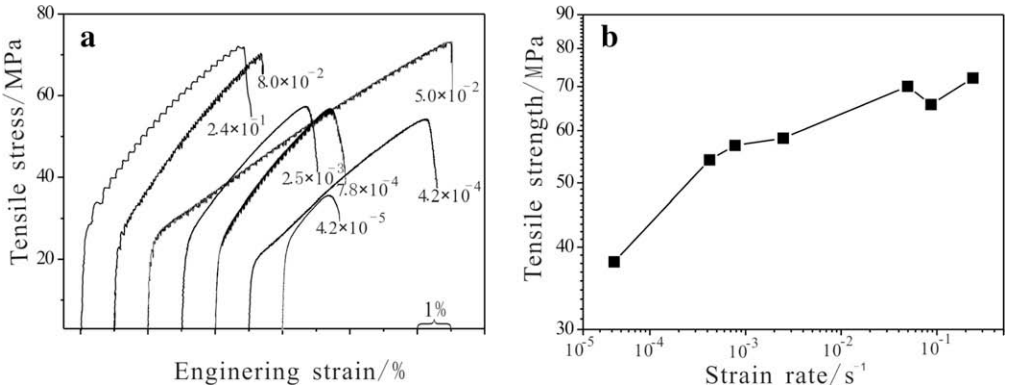

Fig. 5. Tensile stress–strain curves and plot of lg(strain rate)–lg(tensile strength) of Sn–3Cu/Cu joint samples aged at 160 °C for 5 days.

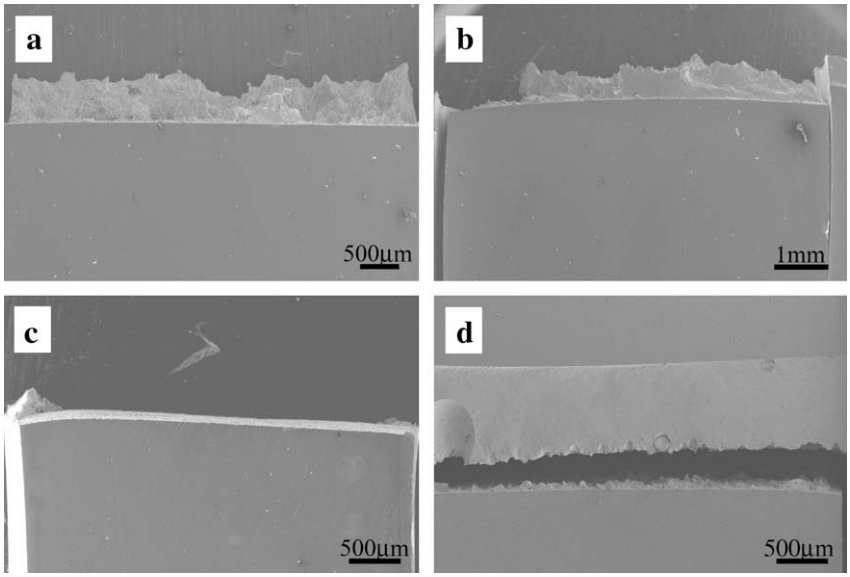

Fig. 6. Cross-section macroscopic tensile fracture morphologies of Sn–3Cu/Cu joint samples aged at 160 °C for 5 days at different strain rates of (a) $4.2 \times 10^{-5}\ s^{-1}$; (b) $2.5 \times 10^{-3}\ s^{-1}$; (c) $5.0 \times 10^{-2}\ s^{-1}$; and (d) $2.4 \times 10^{-1}\ s^{-1}$.

different. It is so flat that little solder can be seen on the IMC side, as illustrated in Figs. 6c and d and 7c and d. These phenomena have been observed under shear loading because the strain rate is always high in the shear test [8,17]. Besides, many slip bands can be observed at the interface, indicating that the Cu substrate took part in the plastic deformation during tension, as displayed by the black arrows in Fig. 7c.

Fig. 8 is the top view of fracture surface of tensile samples aged at 160 °C for 5 days at different strain rates. It can be seen that bulk solder clings to the IMC under low strain rate condition, as displayed in Fig. 8a and b. And also many dimples can be found on the fracture surface, as shown in Fig. 9a and b. It is similar to the fracture surface of the aged samples, as displayed in Fig. 4. In contrast, little solder and many IMCs were detected on the fracture surface under high strain rate condition, as displayed in Fig. 8c and d. Compared with the low strain rate condition, many broken IMCs can be detected on the top view of fracture surface, which has been observed by Lee et al. [17], as shown in Fig. 9c and d. Meanwhile, many broken IMC particles and many parallel cracks were detected on the fracture surfaces, as indicated by the arrows in Figs. 8d and 9c and d. Sometimes, some Cu_3Sn can be also detected near these parallel cracks. The local parallel cracks should result from the impingement of the slip bands in single crystal Cu to the IMC layer because the high tensile stress induced by high strain rates is easy to produce the strong slip bands in Cu single crystal substrate. And then these Cu_3Sn would be impinged from the bottom to the fracture surface, forming some long and straight cracks across the Cu_3Sn and Cu_6Sn_5 grains on the fracture surface (see Figs. 9c and d).

Fig. 10 shows some microstructures under high strain rate condition. It can be seen that the crack firstly initiated at the interface of solder and IMC, as displayed in Fig. 10a. No matter the strain rate

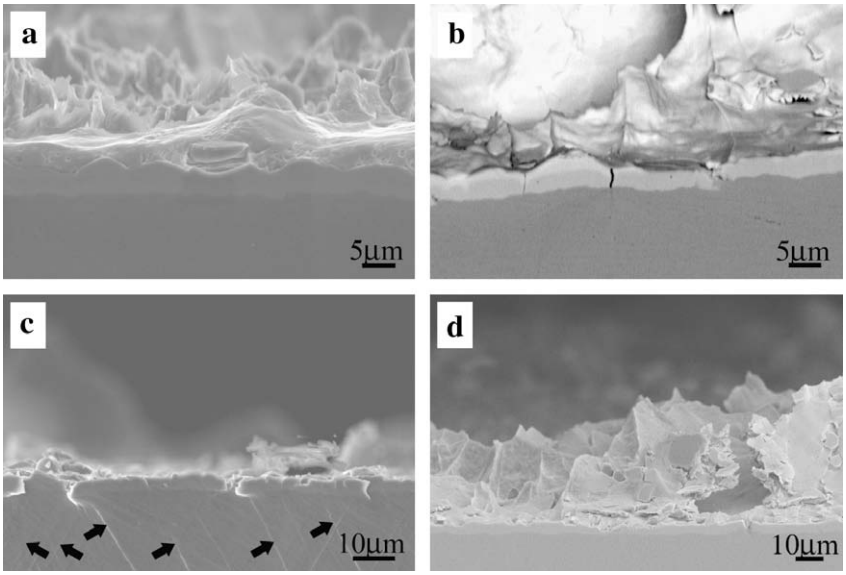

Fig. 7. Cross-section microscopic fracture morphologies on of Sn–3Cu/Cu joint samples aged at 160 °C for 5 days at different strain rates of (a) $4.2 \times 10^{-5}\ s^{-1}$; (b) $2.5 \times 10^{-3}\ s^{-1}$; (c) $5.0 \times 10^{-2}\ s^{-1}$; (d) $2.4 \times 10^{-1}\ s^{-1}$.

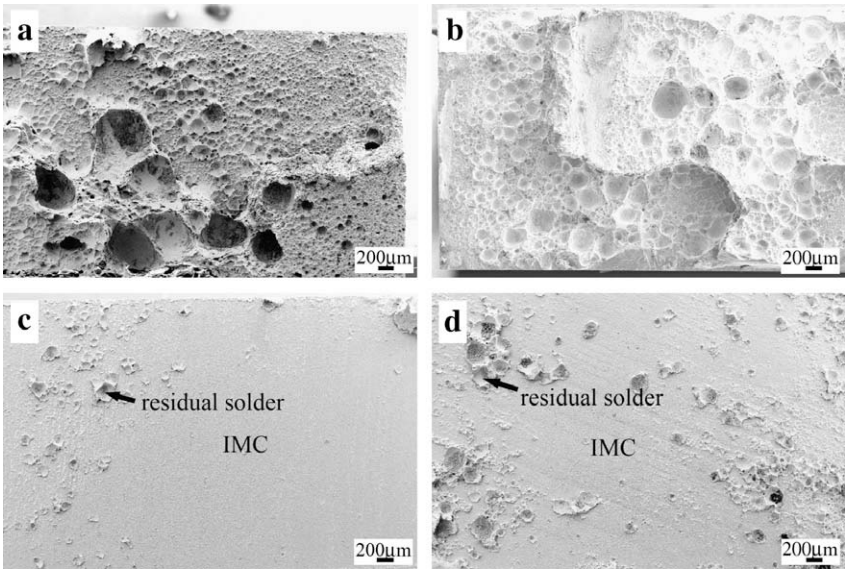

Fig. 8. Top view of tensile fracture surfaces for the samples aged at 160 °C for 5 days at different strain rates: (a) $4.2 \times 10^{-5}\ s^{-1}$; (b) $2.5 \times 10^{-3}\ s^{-1}$; (c) $5.0 \times 10^{-2}\ s^{-1}$; (d) $2.4 \times 10^{-1}\ s^{-1}$.

is low or high, small shear regions can be also detected in the fractography edge of the samples, as illustrated in Fig. 10b. In addition, many parallel cracks are able to be seen on the top view of the fractured samples under high strain rate condition, as illustrated in Fig. 10. Sometimes Cu_3Sn is exposed near these parallel cracks. The reason may be that the shear stress increases high enough to produce the strong slip bands on Cu single crystal substrate at a high strain rate condition. Then IMC layer would be impinged to induce these parallel cracks, as illustrated in Figs. 7c and 10c. Fig. 10d shows the top view of the sample near the solder side under high strain rate condition. Besides many small Sn grains, many broken IMC particles can also be detected on this top view, as illustrated by arrows in Fig. 10d. Similar broken IMCs also appeared on the IMC side, as illustrated in Fig. 9c and d, indicating the occurrence of brittle fracture mode.

According to the observations from Figs. 6–9, it is known that the tensile fracture mode has experienced a great transition from ductile fracture in the low strain rate range (10^{-1} s^{-1}, 10^{-2} s^{-1}) to brittle fracture in the high strain rate range (10^{-3} s^{-1}, 10^{-4} s^{-1}, 10^{-5} s^{-1}). It is assumed that the tensile strength of the joints would change with increasing the strain rate, some researchers found that the relationship between ultimate tensile strength of solder (σ_s) and strain rate ($\dot{\varepsilon}$) can be expressed [23–25]:

$$\sigma_s = C_1 \dot{\varepsilon}^{m_1}, \tag{1}$$

where C_1 is a constant and m_1 is the strain rate sensitivity index of the solder. It is obvious that the data dots do not form a straight line in the total strain rate range, as indicated in Fig. 11. Therefore, the $\lg \sigma_s - \lg \dot{\varepsilon}$ curve in Fig. 11 should be considered to be separated into two parts in the total strain rate range due to the change in the failure manner. In the low strain rate range, the $\lg \sigma_s - \lg \dot{\varepsilon}$ curve should represent the effect of strain rate on tensile strength of the solder itself, which follows Eq. (1). However, since the failure of the joint samples mainly occurred in the IMC layer in the high strain rate

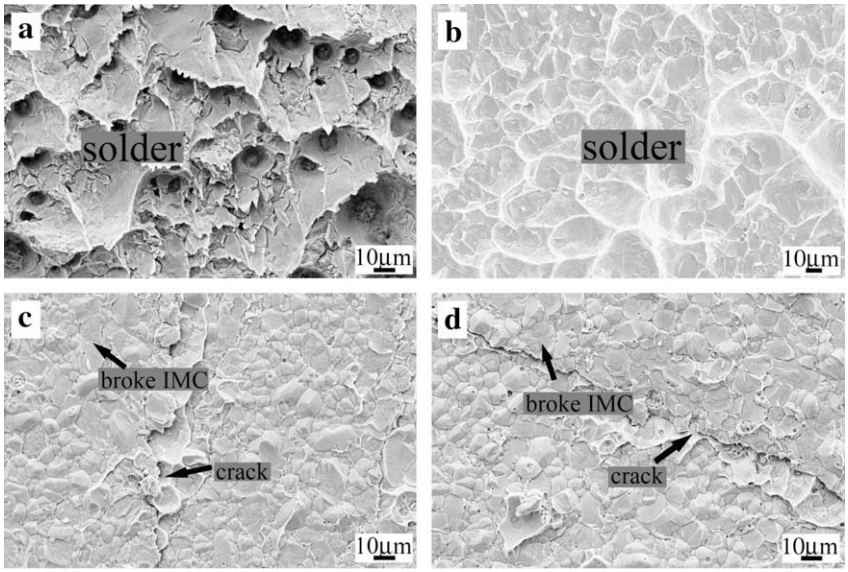

Fig. 9. Tensile fracture morphologies of the samples aged at 160 °C for 5 days at low strain rates: (a) 4.2×10^{-5} s^{-1}; (b) 2.5×10^{-3} s^{-1}; (c) 5.0×10^{-2} s^{-1}; (d) 2.4×10^{-1} s^{-1}.

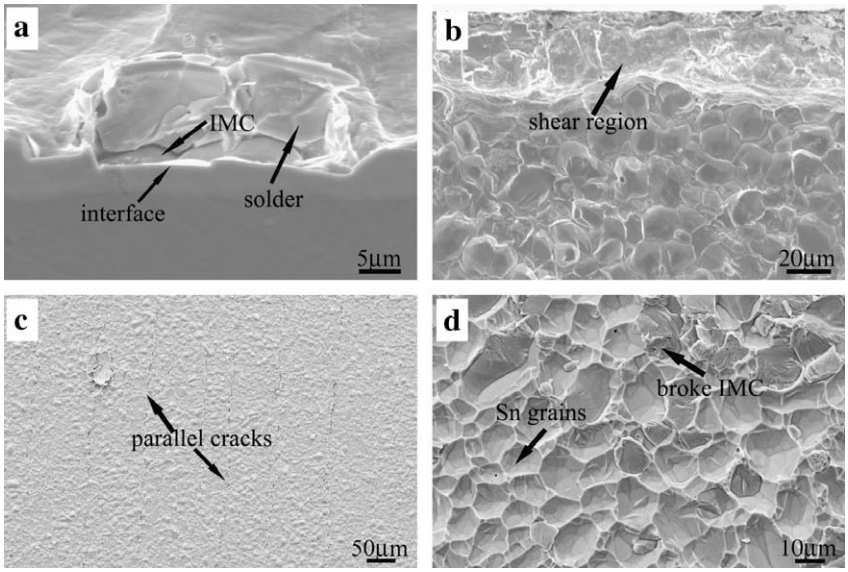

Fig. 10. Tensile fracture morphologies of the samples aged at 160 °C for 5 days at high strain rates: (a), (b), (d) 8.0×10^{-2} s^{-1}; (c) 5.0×10^{-2} s^{-1}.

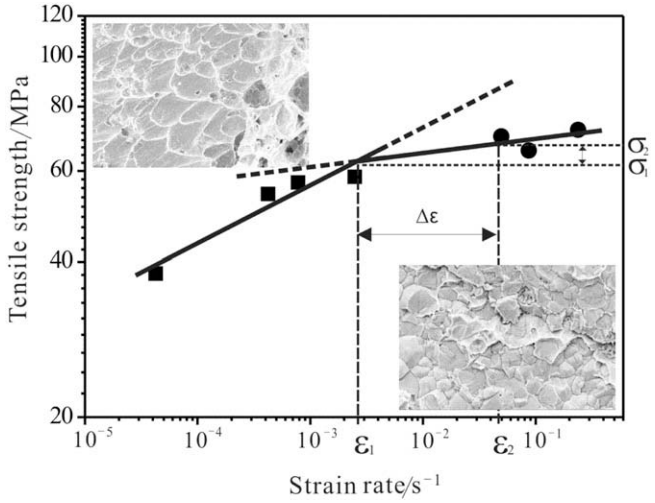

Fig. 11. Plot of the $\lg\sigma - \lg\dot{\varepsilon}$ curves of Sn–3Cu/Cu joint samples aged at 160 °C for 5 days.

range, it is natural to assume that the tensile strength of the IMC layer (σ_i) obeys the similar equation with different constants of C_2 and m_2 as below:

$$\sigma_i = C_2\dot{\varepsilon}^{m_2}, \tag{2}$$

where, C_2 is a constant and m_2 is the strain rate sensitivity index of the IMC layer. According to Eqs. (1) and (2), it is easy to understand why the $\lg\sigma - \lg\dot{\varepsilon}$ curve in Fig. 11 has two different slopes in the total strain rate range because there are two different failure mechanisms, i.e., ductile fracture of solder at low strain rates, as demonstrated by the lower-right corner picture in Fig. 11, and brittle fracture of IMC layer at high strain rates, as illustrated by the upper-left corner picture in Fig. 11. Furthermore, the two values of m_1 and m_2 were calculated from the two slopes of the $\lg\sigma - \lg\dot{\varepsilon}$ curves. It is apparent that m_1 (0.112) of the Sn–3Cu solder is approximately equal to that (0.080) of Sn–3.5Ag solder, but is obviously higher than m_2 (0.026) of the IMC layer [23–25]. This indicates that the tensile strength of the solder is more sensitive to the strain rate than that of the IMC layer.

3.3. Effect of solder thickness on fracture behaviors

Fig. 12a shows the typical tensile stress–strain curves of Sn–3Cu/Cu joints aged at 160 °C for 15 h. The tensile strength of the thinner samples is higher than that of the thicker samples, but the tensile strain of the thick samples is larger than that of the thinner samples. Fig. 12b shows the dependence of the tensile strength on the solder thickness. These data indicate that the tensile strength would decrease with increasing the solder thickness. In fact, Saxton, West and Barret [26,27] have investigated the failure of the brazed joints with different braze thickness. Interpretation of their experimental results in terms of the Orowan expression for joint strength is as below:

$$\sigma_F = \sigma_{UTS/yield}(\text{braze or solder}) \times (1 + d/6t) \tag{3}$$

where σ_F is the joint fracture strength and $\sigma_{UTS/yield}$ is the yield strength or fracture strength of the brazing metal (in our experiment, the brazing metal is Sn3Cu alloy, then $\sigma_{UTS/yield}$ should be the fracture strength of the Sn3Cu solder), t means the solder thickness of the joint and d is the diameter of samples. Based on these results, the Orowan theory should be also valid for solder joints. In Orowan's approximation the geometry of the tensile specimen was chosen to be cylindrical but our results showed a quite similar behavior for the rectangular shaped joints (recalculated for a similar area). Then the Orowan theory curve can be obtained (experimentally determined the fracture strength of the used Sn3Cu to be 28 MPa), as presented by the solid curve in Fig. 12b. It is close to our experimental results, as illustrated in Fig. 12b.

Fig. 13 shows the tensile fracture morphologies of SnCu/Cu joint with thicker solder (about 1339 μm). Normally, the joints with thicker solder present ductile deformation behavior, as demonstrated by Figs. 12a and 13a. Fig. 13b shows the cross-section and the top view of the fracture interface. It is indicated that the fracture basically occurred along the Cu–Sn IMC/SnCu solder interface, which is similar to many solder joints [28]. Fig. 13d shows the magnified morphology of the fracture surface, and many dimples were detected on the fracture surface. This further confirms that the SnCu/Cu joint with thicker solder would break in a ductile manner.

Compared with the joint with thick solder, the fracture surface of the joint with thinner solder is different from that of the joint with thick solder. Fig. 14 shows the fracture surface of the joint with thin solder. It is found that the joint with thinner solder broke in a brittle manner, as demonstrated in Figs. 12a and 14a. According to Fig. 14b, the fracture basically occurred along the Cu–Sn IMC. This is why low elongation was observed from the joint with thin solder. Fig. 14c and d shows the top view of the fracture surface of the joint with thin solder and many Cu–Sn IMCs can be detected from the top view.

Based on the above analysis, it can be concluded that the solder joints broke in a ductile manner and presented a low tensile strength for the joint with thicker solder, but displayed a brittle manner and a higher tensile strength for the joint with thinner solder, as illustrated in Fig. 12b. Therefore, solder thickness plays an

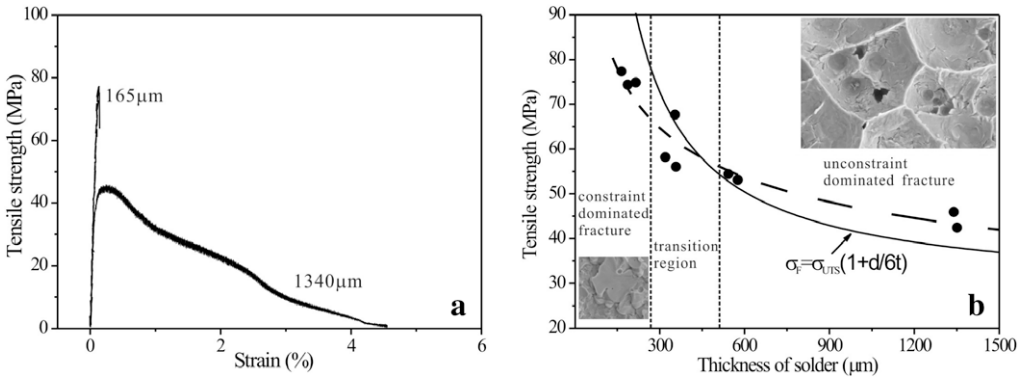

Fig. 12. (a) Tensile stress–strain curves of SnCu/Cu joint with different solder thickness; (b) the dependence of the tensile strength on the solder thickness.

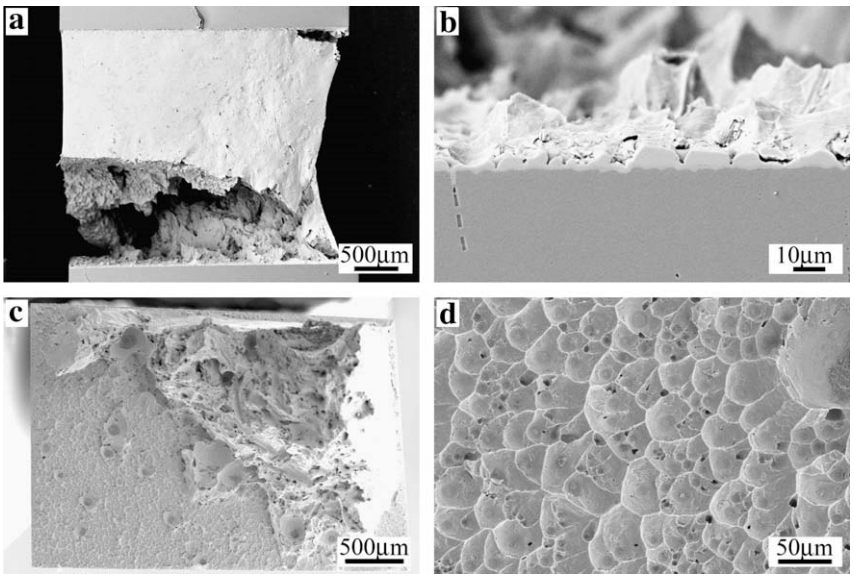

Fig. 13. Tensile fracture morphologies of SnCu/Cu joint with thick solder: (a) and (b) cross-section of the fracture; (c) and (d) the top view of fracture surface.

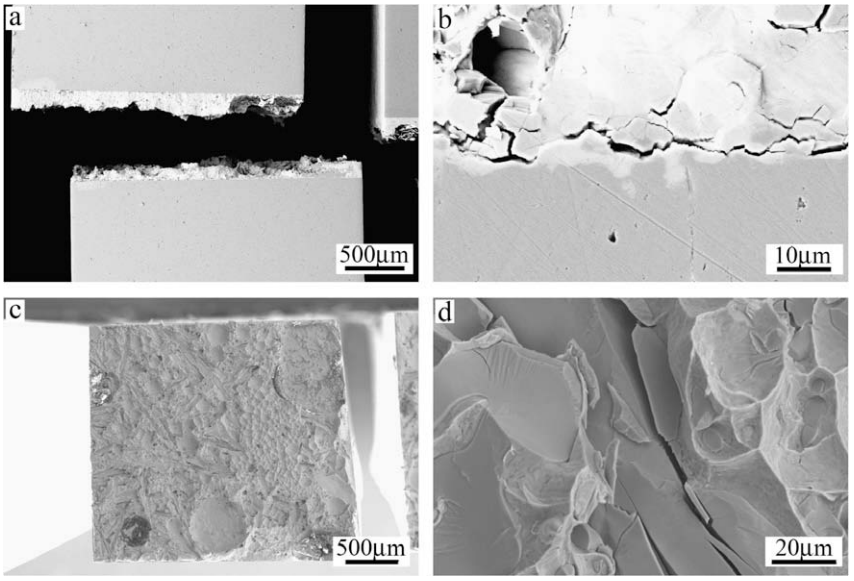

Fig. 14. Tensile fracture morphologies of SnCu/Cu joint with thin solder: (a) and (b) cross-section of the fracture; (c) and (d) the top view of fracture surface.

important role in the fracture behavior and the interfacial mechanical properties.

4. Conclusions

The fracture behaviors of Sn–3Cu/Cu joint have been investigated under different conditions, including aging time, strain rate and solder thickness. Based on these experimental results, the following conclusions can be drawn.

1. With increasing aging time, the tensile strength of joint has a slight decreasing tendency, and their fracture modes are nearly the same.
2. With increasing strain rate, the tensile strength of joint has an intense increasing tendency. Meanwhile, in those tests, the ductile-to-brittle transition was observed with increasing strain rate. Under low strain rate condition, the fracture mainly occurs in the solder; however, the fracture location is changed into the IMC or the interface between IMC and solder under high strain rate condition.
3. When the solder thickness is very thin, the samples broke in a brittle manner; and many big broken IMCs can be detected on the fracture surface. For the joint with thick solder, the fracture mode is changed from brittle-to-ductile manner. More solder and dimples can be found on the fracture surface.

Acknowledgements

The authors would like to thank Q.Q. Duan, W. Gao, P. Li, H.H. Su and Q.S. Zhu for mechanical tests and SEM observations. This work was financially supported by National Basic Research Program of China under Grant No. 2004CB619306, 2010CB631006 and the National Outstanding Young Scientist Foundation under Grant No. 50625103.

References

[1] M. Abtew, G. Selvaduray, Mater. Sci. Eng. R 27 (2000) 95–145.
[2] X. Gu, Y.C. Chan, J. Electron. Mater. 37 (2008) 1721–1726.
[3] S.J. Jeon, S. Hyun, H.J. Lee, et al., Microelectron. Eng. 85 (2008) 1967–1970.
[4] C.W. Chang, C.E. Ho, S.C. Yang, C.R. Kao, J. Electron. Mater. 35 (2006) 1948–1954.
[5] F.Q. Yang, L.L. Peng, K.J. Okazaki, J. Mater. Res. 21 (2006) 2653–2659.
[6] J.S. Lee, K.M. Chu, R. Patzelt, et al., Microelectron. Eng. 85 (2008) 1577–1583.
[7] F.L. Zhu, H.H. Zhang, R.F. Guan, S. Liu, Microelectron. Eng. 84 (2007) 144–150.
[8] B.Y. Wu, H.W. Zhong, Y.C. Chan, M.O. Alam, J. Mater. Res. 21 (2006) 2224–2231.
[9] A. Fawzy, Mater. Charact. 58 (2007) 323–331.
[10] F.J. Wang, X. Ma, Y.Y. Qian, Scripta Mater. 53 (2005) 699–704.
[11] C.H. Wang, S.W. Chen, Acta Mater. 54 (2006) 247–253.
[12] J.W. Yoon, S.W. Kim, J. Alloys Compd. 391 (2005) 82–89.
[13] F. Ren, J.W. Nah, K.N. Tu, Appl. Phys. Lett. 89 (2006) 141914.
[14] H.T. Lee, M.H. Chen, Mater. Sci. Eng. A. 333 (2002) 24–34.
[15] K.S. Bae, S.J. Kim, J. Mater. Res. 17 (2002) 743–746.
[16] H.F. Zou, H.J. Yang, Z.F. Zhang, Acta Mater. 56 (2008) 2649–2662.
[17] H.T. Lee, M.H. Chen, H.M. Jao, T.L. Liao, Mater. Sci. Eng. A. 358 (2003) 134–141.
[18] D.G. Kim, J.W. Kim, S.B. Jung, Mater. Sci. Eng. B 121 (2005) 204–210.
[19] Y.H. Xia, X.M. Xie, C.Y. Lu, J.L. Chang, J. Alloys Compd. 417 (2006) 143–149.
[20] D.Q. Yu, C.M.L. Wu, C.M.T. Law, L. Wang, J.K.L. Lai, J. Alloys Compd. 392 (2005) 192–199.
[21] L. Pang, S.M. Han, K.S. Kumar, Acta Mater. 50 (2002) 3623–3639.
[22] L. Pang, K.S. Kumar, Acta Mater. 46 (1998) 4017–4028.
[23] F. Lang, H. Tanaka, O. Munegata, T. Taguchi, T. Narita, Mater. Charact. 54 (2005) 223–229.
[24] I. Shohji, T. Yoshida, T. Takahashi, S. Hioki, Mater. Sci. Eng. A 366 (2004) 50–55.
[25] H.F. Zou, Z.F. Zhang, J. Mater. Res. 23 (2008) 1614–1617.
[26] H.J. Saxton, A.J. West, C.R. Barrett, Met. Trans. 2 (1971) 999–1007.
[27] A.J. West, H.J. Saxton, A.S. Tetelman, C.R. Barrett, Met. Trans. 2 (1971) 1009–1017.
[28] H.F. Zou, Q.S. Zhu, Z.F. Zhang, J. Alloys Compd. 461 (2008) 410–417.